

---

# Improving Generative Adversarial Networks with Self-Distillation

---

**Antoni Nowinowski**  
 Poznan University of Technology  
 antoni.nowinowski@cs.put.poznan.pl

**Krzysztof Krawiec**  
 Poznan University of Technology  
 krzysztof.krawiec@cs.put.poznan.pl

## Abstract

In modern GANs, maintaining an Exponential Moving Average (EMA) of the generator’s weights is a standard practice, as such an averaged model consistently outperforms the actively trained generator. However, the EMA generator is used for final deployment only and does not influence the training process. To address this missed opportunity, we introduce Self-Distilled GAN (SD-GAN) that employs the EMA generator as a teacher to guide the active generator (student) via perceptual loss. We prove the local asymptotic stability of SD-GAN in the Dirac-GAN setting and show that it dampens the parasitic cycling behavior that plagues conventional GANs. Empirical evaluations across established architectures and datasets demonstrate that SD-GAN improves the final image quality on several metrics (FID and random-FID in particular), stabilizes the optimization trajectory and provides additional learning guidance that is not trivially correlated with the conventional adversarial loss. It also proves effective for fine-tuning pretrained GAN models.

## 1 Introduction

Obtaining well-performing generators by training generative adversarial networks (GANs) [1] can be notoriously challenging, one reason being that the game played between the generator ( $G$ ) and the discriminator ( $D$ ) tends to engage in a cyclic “chase” or entirely fail to converge [2]. The resulting  $G$  may then fail to capture the entirety of the distribution represented by the training sample or produce samples of inferior quality. To address this challenge, it is common to obtain final generators from GANs using weight averaging, which is typically performed outside or inside the training loop. In the former case, the averaged model is kept “on the side” and does not influence the training process in any way, being used only for the post-training evaluations, e.g., in stochastic weight averaging [3]. In the latter case, the averaged model is used as a teacher in self-distillation (SD) student-teacher mode, as in Mean Teachers [4], BYOL [5], and the DINO family of models [6, 7, 8]. In most of those scenarios, it is common to aggregate the models using exponential moving average (EMA), which naturally attributes more importance to the more recent models. Specifically, at each training step  $t$ , the EMA weights  $\theta_{EMA}$  are updated using the weights  $\theta$  of the active model at decay rate  $\beta$ :

$$\theta_{EMA}^{(t)} = \beta\theta_{EMA}^{(t-1)} + (1 - \beta)\theta^{(t)}. \quad (1)$$

In this study, we propose Self-Distilled GAN (SD-GAN) that incorporates SD into GAN training (Fig. 1): rather than learning from the adversarial loss alone, the generator  $G$  also learns from its self-distilled teacher  $G_{EMA}$  obtained from  $G$  using EMA. To this end,  $G$  and  $G_{EMA}$  are queried on the same latent vector and the similarity of the images they produce is assessed using a popular form of perceptual loss (LPIPS, [9]). This changes the training trajectory of  $G$ , and subsequently the discriminator  $D$ . We show that this extension of the traditional GAN paradigm stabilizes training, makes it faster and ultimately results in generators that produce more realistic images.

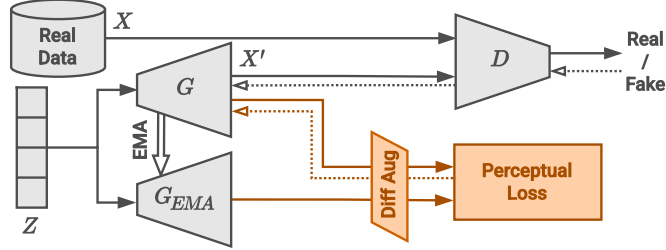


Figure 1: Overview of the SD-GAN framework. The training is guided by both the conventional GAN loss and the self-distillation loss. Dotted lines indicate gradient flow; gradients from the perceptual loss do not propagate through  $G_{EMA}$ .

## 2 Related Work

**Weight averaging in GANs.** An early attempt to stabilize GAN training by leveraging the historical states of the players was *historical averaging* [10], which penalized both  $G$  and  $D$  by the distance between the current and the historical parameters, defined as  $\|\theta^{(t)} - \frac{1}{T} \sum_{i=1}^T \theta^{(t-i)}\|^2$ . However, it neither maintains a shadow generator for inference nor uses exponential discounting.

To our knowledge, maintaining an EMA of the weights of a GAN generator was first introduced as part of the Progressive Growing of GANs (ProGAN) training framework [11]. In order to maintain the generator’s responsiveness, the authors opted not to use learning rate decay. Consequently, the weights fluctuated significantly during training, leading to visual artifacts. To dampen this variance and produce stable outputs, they maintained a passive EMA of the generator’s weights.

The above techniques were introduced as practical engineering heuristics to improve inference quality, without theoretical justification or citations to the prior literature. To bridge this gap, Yazici et al. [12] conducted a formal analysis of weight averaging in GANs. They noted that standard gradient descent in adversarial minimax games frequently fails to converge, as the players continuously orbit the optimal solution in limit cycles. Through a theoretical analysis, they proved that while EMA does not directly achieve the Nash equilibrium, it exponentially shrinks the amplitude of these limit cycles. Consequently, the active  $G$  model continues exploring the loss landscape, while the passive  $G_{EMA}$  is confined to the neighborhood of the equilibrium point. Extensive empirical evaluations confirmed that EMA models consistently achieve higher image fidelity than their actively trained counterparts. This dynamic has also been studied in [13] across a set of image classification tasks, revealing that EMA models reliably converge to fundamentally different, flatter basins of the loss landscape, not only improving final generalization but yielding remarkable early-stage performance, largely explaining their success when used as teachers.

Following the introduction in ProGAN, EMA of generator weights became a standard component of most state-of-the-art generative models. The technique was adopted in BigGAN [14], the StyleGAN lineage of models [15, 16, 17, 18], ProjectedGAN [19], StyleGAN-XL [20], StyleGAN-T [21], SAN [22], and StyleNAT [23], as well as in diffusion models [24, 25, 26]. However, in contrast to SD-GAN, in all these architectures,  $G_{EMA}$  serves as the end-of-run outcome, while not directly impacting the training process.

**Stabilization and consistency regularization.** Alongside weight averaging, various regularization techniques have been proposed to stabilize the adversarial game. For instance, CR-GAN [27] and bCR [28] apply consistency terms to the discriminator, penalizing prediction changes across differently augmented views of the same image, while methods like DiffAugment [29] apply differentiable augmentations to both real and fake samples to prevent discriminator overfitting. On the generator side, latent consistency regularization (zCR) [28] maximizes the difference between images generated from perturbed latent codes to promote diversity. Furthermore, LeCam regularization [30] utilizes discriminator EMA to anchor its predictions to historical states. While these methods are highly effective, they predominantly prevent discriminator overfitting or enforce latent consistency. In contrast, SD-GAN introduces temporal consistency directly into the generator’s trajectory.

**Knowledge distillation.** In the modern generative landscape, knowledge distillation is widely utilized, though predominantly to improve computational efficiency rather than training stability. This includes

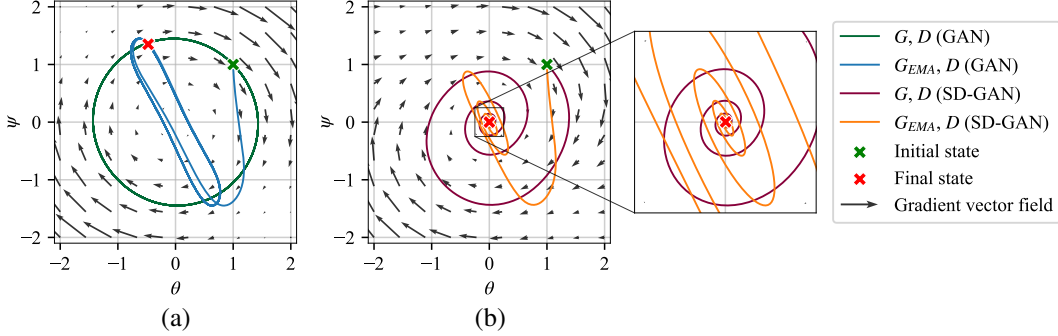


Figure 2: Parameter trajectories of the active generator ( $\theta$ ), EMA generator ( $\theta_{EMA}$ ) and discriminator ( $\psi$ ) in the Dirac-GAN. **(a)** Standard GAN forms cycles orbiting the Nash equilibrium. **(b)** Self-distillation dampens these cycles into a contracting spiral. The gradient vector field (b) is evaluated for the final  $\theta_{EMA}$ .

distilling lightweight student GANs from larger teacher models [31, 32]. Concurrently, adversarial distillation techniques have been applied to diffusion models to reduce inference times, enabling high-fidelity sampling in a few steps [33, 34] or a single step [35]. Beyond model compression, some elements of self-distillation combined with GANs have also been used as a component for a specific supervised downstream task [36]. In contrast, SD-GAN utilizes it to directly improve the primary model’s training trajectory and final image quality. Recently, consistency models [37], a new class of diffusion-inspired generative models, have similarly demonstrated the efficacy of EMA-based self-distillation, utilizing a slowly updated target network as a stable reference to guide the active model. Finally, SD-GAN should not be confused with Self-Distilled StyleGAN [38], as the latter focuses on generative self-filtering to curate noisy, multi-modally distributed web data.

### 3 Self-Distilled GAN

The motivation for SD-GAN is similar to that postulated in previous methods that engaged weight averaging and self-distillation [4]: (i) to provide the learner (student) with a form of long-term memory (the teacher) that integrates the effects of the learning process, and (ii) to use the teacher as an anchor to stabilize the training, i.e. to avoid catastrophic forgetting of the already acquired knowledge, while allowing for a fair share of exploration. To that aim, we extend the traditional GAN adversarial loss function with a self-distillation loss applied to the outputs of the active generator model  $G$  and the averaged model  $G_{EMA}$ . Specifically,  $G$  and  $G_{EMA}$  are queried on the same random latent vector  $z$ , and the images they produce are compared using an SD loss component  $\mathcal{L}_{SD}$ . The gradient calculated from  $\mathcal{L}_{SD}$  affects only  $G$ , i.e.  $G_{EMA}$  is updated only via EMA (Fig. 1).

In general,  $\mathcal{L}_{SD}$  can be any image-comparing loss; however, we demonstrate in Sec. 4 that perceptual loss functions provide the greatest advantage for SD-GAN. Specifically, we utilize LPIPS [9], which evaluates the distance between the feature activations of the two images when passed through a pretrained network. Before the similarity between the generated images is evaluated, both outputs are subjected to the exact same sequence of differentiable augmentations  $T$  (random spatial transformations, see Appendix C). The final objective function for the generator is a weighted sum of the standard adversarial loss  $\mathcal{L}_{adv}$  and  $\mathcal{L}_{SD}$ :

$$\mathcal{L}_G = \mathcal{L}_{adv} + \alpha \cdot \mathcal{L}_{SD}(T(G(z)), T(G_{EMA}(z))) \quad (2)$$

where  $\alpha$  controls the weight of the guidance provided by the EMA teacher.

**Theoretical intuition.** To better understand the stabilizing mechanism of SD-GAN, we analyze its behavior on the Dirac-GAN [2], a simple, one-dimensional model used to study the convergence of GANs. The Dirac-GAN consists of a true data distribution fixed at zero, a generator modeled as a constant function with a single learnable parameter  $G(z) = \theta$ , and a linear discriminator  $D(x) = \psi \cdot x$ . Consequently, the discriminator’s score on generated data is  $D(G(z)) = \psi\theta$ , and the adversarial loss takes the form  $\mathcal{L}_{adv} = f(\psi\theta)$  (where  $f$  is determined by the GAN variant; here  $f$  is identity). The unique Nash equilibrium of this system is  $(\theta^*, \psi^*) = (0, 0)$ .

Figure 2 illustrates the trajectories of these parameters during training. In the basic GAN (2a, green plot), gradient descent does not converge, with  $G$  and  $D$  persistently orbiting the equilibrium; incorporating EMA (blue plot) narrows the orbit, but does not improve convergence. The right inset (2b) demonstrates the dynamics when extending these configurations with our self-distillation objective  $\mathcal{L}_{SD}$  (simplified to  $\alpha(G(z) - G_{EMA}(z))^2$ ). By continuously penalizing the distance between the active generator and the EMA generator,  $\mathcal{L}_{SD}$  introduces a damping force that transforms the circular, non-converging trajectory into a contracting spiral, forcing the parameters to converge in the limit to the exact Nash equilibrium. This happens both for the EMA (orange) and the non-EMA (indigo) configuration. This analytical model corroborates our empirical findings: by anchoring the active model to its historical average, SD-GAN mitigates oscillatory training dynamics and ensures stable convergence.

**Proof of convergence.** We follow the above intuition with a more rigorous formalization by examining the gradient vector field and deriving the exact local convergence criterion. As in prior analyses of local GAN stability, we study the continuous-time dynamics through the spectrum of the Jacobian of the vector field at the equilibrium [39, 40, 41, 2]. We consider a continuous-time formulation of the Dirac-GAN minimax game. We denote the active generator parameter as  $\theta(t)$ , the discriminator parameter as  $\psi(t)$ , and the EMA generator parameter as  $\phi(t)$  (rather than  $\theta_{EMA}(t)$ , for brevity), and introduce continuous-time learning rates  $\eta_G, \eta_D > 0$  for the generator and discriminator respectively. For the adversarial objective  $\mathcal{L}_{adv}(\theta, \psi) = f(\psi\theta)$ , the local behavior near the Nash equilibrium depends only on  $c = f'(0)$ , with  $c \neq 0$ , so we work with the linearized loss function  $\mathcal{L}_{adv} = c\psi\theta$ . The self-distillation penalty is  $\alpha \cdot \mathcal{L}_{SD} = \frac{\alpha}{2}(\theta - \phi)^2$  (the  $\frac{1}{2}$  factor is for convenience). We parametrize the EMA decay rate  $\beta$  as an update rate  $\eta_\phi = 1 - \beta$ . The joint vector field is therefore:

$$\begin{cases} \frac{d\theta}{dt} = -\eta_G(c\psi + \alpha(\theta - \phi)) \\ \frac{d\psi}{dt} = \eta_D c\theta \\ \frac{d\phi}{dt} = \eta_\phi(\theta - \phi) \end{cases} \quad (3)$$

To analyze local stability around the Nash equilibrium  $(\theta^*, \psi^*, \phi^*) = (0, 0, 0)$ , we construct the Jacobian matrix  $J$  of the state vector  $(\theta, \psi, \phi)$ :

$$J = \begin{bmatrix} -\eta_G\alpha & -\eta_Gc & \eta_G\alpha \\ \eta_Dc & 0 & 0 \\ \eta_\phi & 0 & -\eta_\phi \end{bmatrix} \quad (4)$$

The system converges asymptotically to the Nash equilibrium if and only if all eigenvalues  $\lambda$  of  $J$  have negative real parts [39]. We solve the characteristic equation  $\det(\lambda I - J) = 0$  by expanding along the second row:

$$\lambda^3 + (\eta_G\alpha + \eta_\phi)\lambda^2 + (\eta_D\eta_Gc^2)\lambda + \eta_D\eta_G\eta_\phi c^2 = 0 \quad (5)$$

To make sure the eigenvalues  $\lambda$  have negative real parts, we apply the Routh–Hurwitz criterion [39], which states that all roots of a 3rd-degree polynomial ( $a_3\lambda^3 + a_2\lambda^2 + a_1\lambda + a_0 = 0$ ) will have strictly negative real parts if and only if (i)  $a_3, a_2, a_1, a_0 > 0$  and (ii)  $a_2a_1 > a_3a_0$ :

$$\begin{aligned} \text{(i)} \quad & a_3: 1 > 0 & a_2: \eta_G\alpha + \eta_\phi > 0 & \text{(ii)} \quad \eta_D\eta_G^2c^2\alpha > 0 \\ & a_1: \eta_D\eta_Gc^2 > 0 & a_0: \eta_D\eta_G\eta_\phi c^2 > 0 & \end{aligned} \quad (6)$$

Because the learning rates  $\eta_G, \eta_D > 0$ , the condition simplifies to  $\alpha > 0$ . Therefore, for any valid learning rates  $\eta_G, \eta_D > 0$ , and EMA decay rate  $\beta \in [0, 1)$ , introducing a self-distillation penalty  $\alpha > 0$  strictly guarantees that the eigenvalues have negative real parts, proving local asymptotic convergence to the exact Nash equilibrium, rather than the purely oscillatory behavior of the unregularized Dirac-GAN [2].

## 4 Results

We validate SD-GAN by applying it to the well-established GAN architectures StyleGAN2-ADA [17], ProjectedGAN [19] and StyleNAT [23], and experimenting with the widely used benchmarks FFHQ [15] and LSUN Church [42] at  $256^2$  resolution. We take care to faithfully reproduce the architectures and results of the cited works by relying on the original implementations (including metric calculation), and amending them only as minimally as required to extend them to SD-GAN.

See Appendix A for further details. Despite our best efforts, we did not manage to replicate the results of StyleNAT on LSUN Church sufficiently well, so we discard this combination (see Appendix B for details). In addition to the default version of SD-GAN that uses LPIPS as  $\mathcal{L}_{SD}$ , we also consider a simplified variant that uses pixel-wise  $L_1$  for that purpose. We set  $\alpha = 1$  for StyleGAN2-ADA and ProjectedGAN and  $\alpha = 0.25$  for StyleNAT (as its  $\mathcal{L}_{adv}$  is roughly  $4\times$  smaller on average).

Similar to other works, we use the Fréchet Inception Distance (FID, [43]) as the primary metric for measuring the quality of obtained generators. The FID estimates are calculated from a sample of 50k generated images and compared against the full dataset. However, to address the growing criticism regarding its vulnerability to ImageNet-specific biases [20, 44], we complement it with the random-FID (rFID, [20]). By employing an untrained feature extractor, rFID helps verify if improvements on FID result from fundamental gains in image quality rather than metric-specific artifacts. Furthermore, to rigorously test whether the self-distillation objective induces mode collapse or reduces diversity, we use Precision and Recall [45]. All reported results concern the EMA models.

Figure 3 presents the FID over training effort expressed in thousands of processed real images (kimgs). SD-GAN systematically achieves better FID values (notice log scale), and for the convolutional architectures (StyleGAN2-ADA and ProjectedGAN) does so already from the early iterations of learning. For ProjectedGAN, SD-GAN using LPIPS achieves the same FID as the baseline method at a fraction of the cost ( $\sim 32\%$  on FFHQ and  $\sim 39\%$  on LSUN Church). Using  $L_1$  as  $\mathcal{L}_{SD}$  leads to somewhat worse results than LPIPS, however, usually still better than the baseline. Notably, the curves look smoother for SD-GAN, suggesting that rather than slowing exploration or over-anchoring to the historical state, the distillation objective acts as a stabilizing force, corroborating the theoretical findings from Sec. 3.

Table 1 compares the final metrics achieved by reference methods and their SD-GAN variants. As we observed rFID to vary significantly across independent evaluations due to random feature projection inherent to this metric [20], we compute it five times and report means and standard deviations. The advantage of self-distillation is particularly prominent on this metric, especially for the LPIPS-based SD-GAN; e.g., the ProjectedGAN’s rFID drops from  $79.3 \pm 7.6$  to  $14.1 \pm 2.1$  on FFHQ. This indicates that the guidance provided by the EMA teacher yields improvements that generalize robustly, even when evaluated using an untrained feature extractor (in contrast to the ImageNet-biased FID). When applied to StyleGAN2-ADA and ProjectedGAN, SD-GAN also tends to improve Recall or Precision, while only moderately deteriorating the other metric, demonstrating that the model maintains diversity and, contrary to potential concerns, is not overly anchored to the averaged state by self-distillation. While SD-GAN yields consistent benefits for convolutional baselines, we observe a slight FID regression for the transformer-based StyleNAT (2.17 to 2.27 on FFHQ), despite initial gains visible in Figure 3, suggesting that attention-based architectures may interact differently with the distillation objective, or require further tuning of the hyperparameters.

Table 2 presents the training times and relative computational overheads of training SD-GAN on a single GPU. See Appendix A for the details on our computational infrastructure.

#### 4.1 SD-GAN as a fine-tuning technique

Motivated by the significant computational overheads reported in Table 2, we attempt to engage SD-GAN as a fine-tuning technique. Given a pretrained GAN model, we initialize  $G$ ,  $G_{EMA}$  and  $D$  with the pretrained weights and continue training using a combination of the standard adversarial loss ( $\mathcal{L}_{adv}$ ) and our self-distillation loss ( $\mathcal{L}_{SD}$ ). Figure 4 juxtaposes this with the baseline scenario, which continues training with  $\mathcal{L}_{adv}$  only. In Fig. 4a we fine-tune the StyleGAN2-ADA<sup>1</sup> authors’ official checkpoint of the model trained on FFHQ at  $1024^2$  resolution [17], and subject it to training on the same dataset. SD-GAN quickly improves on FID, proving its efficacy even on megapixel-scale images, while the baseline does not show clear signs of progress. In Fig. 4b we examine a more realistic fine-tuning scenario, starting from the FFHQ at  $256^2$  checkpoint<sup>1</sup> and fine-tuning it on the train split of CelebA-HQ dataset at  $256^2$  [46, 11]. The change of training distribution causes all three models to start from moderate FID values, but they rapidly adapt. Both SD variants not only stabilize the fine-tuning process but also converge to a lower final FID.

<sup>1</sup>Technically we use the StyleGAN2 checkpoints, as recommended in the official repository.

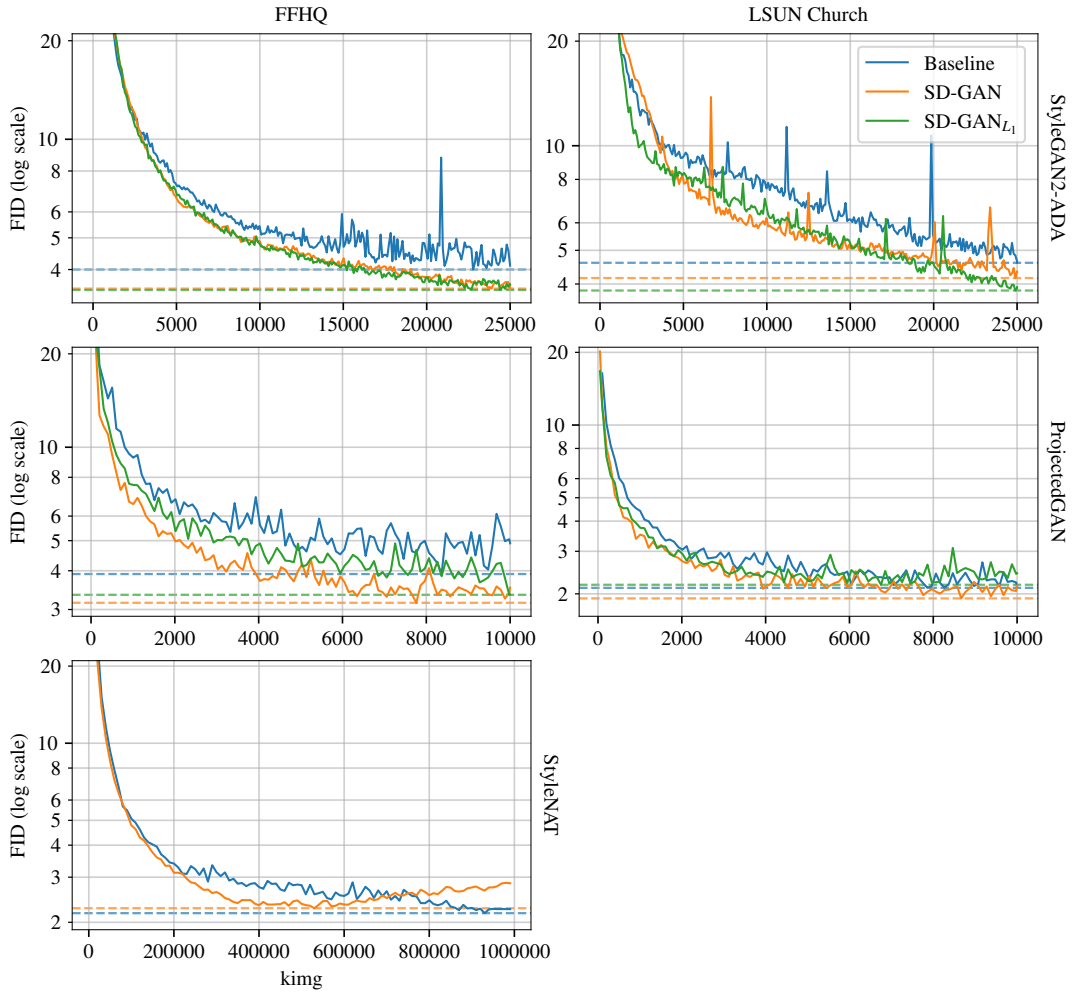


Figure 3: FID scores (log scale) during training on the FFHQ and LSUN Church datasets across three baseline architectures. Following [23], we allowed the StyleNAT to learn much longer than the remaining architectures. Horizontal dashed lines indicate the best FID score.

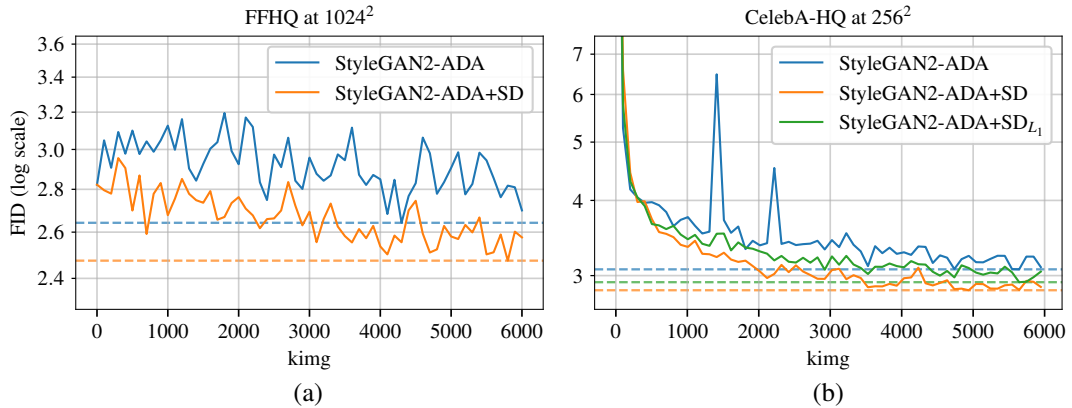


Figure 4: FID scores during fine-tuning on the FFHQ at 1024<sup>2</sup> and CelebA-HQ at 256<sup>2</sup>.

Table 1: Comparison of evaluation metrics (FID, rFID, Precision, and Recall) on FFHQ and LSUN Church datasets at 256<sup>2</sup>. Values in parentheses indicate the original reported scores from the respective papers (see Appendix B for explanations of the discrepancies between them and our results).

| Dataset     | Model                                     | FID ↓       | rFID ↓        | Precision ↑ | Recall ↑ |
|-------------|---|-------------|---------------|-------------|----------|
| FFHQ        | StyleGAN2-ADA                             | 4.00 (4.30) | 1.58 ± 0.11   | 0.692       | 0.399    |
|             | StyleGAN2-ADA+SD                          | 3.50        | 1.18 ± 0.27   | 0.678       | 0.440    |
|             | StyleGAN2-ADA+SD <sub>L<sub>1</sub></sub> | 3.46        | 4.51 ± 0.90   | 0.679       | 0.469    |
|             | ProjectedGAN                              | 3.90 (3.39) | 79.3 ± 7.6    | 0.662       | 0.439    |
|             | ProjectedGAN+SD                           | 3.15        | 14.1 ± 2.1    | 0.666       | 0.452    |
|             | ProjectedGAN+SD <sub>L<sub>1</sub></sub>  | 3.35        | 34.4 ± 3.6    | 0.669       | 0.446    |
|             | StyleNAT                                  | 2.17 (2.05) | 6.31 ± 0.55   | 0.698       | 0.383    |
|             | StyleNAT+SD                               | 2.27        | 4.22 ± 0.70   | 0.676       | 0.367    |
| LSUN Church | StyleGAN2-ADA                             | 4.60        | 2.73 ± 0.18   | 0.626       | 0.218    |
|             | StyleGAN2-ADA+SD                          | 4.16        | 1.81 ± 0.20   | 0.619       | 0.274    |
|             | StyleGAN2-ADA+SD <sub>L<sub>1</sub></sub> | 3.83        | 0.977 ± 0.075 | 0.622       | 0.321    |
|             | ProjectedGAN                              | 2.11 (1.59) | 5.7 ± 1.3     | 0.561       | 0.474    |
|             | ProjectedGAN+SD                           | 1.91        | 1.92 ± 0.28   | 0.605       | 0.446    |
|             | ProjectedGAN+SD <sub>L<sub>1</sub></sub>  | 2.18        | 2.95 ± 0.46   | 0.607       | 0.429    |

Table 2: Computational requirements of SD-GAN training compared to the baseline methods: the time (in seconds) required to process 1 kimg and the average memory consumption.

| Method                                    | StyleGAN2-ADA |         | ProjectedGAN |         | StyleNAT |         |
|---|---------------|---------|--------------|---------|----------|---------|
|   | s/kimg        | Mem.    | s/kimg       | Mem.    | s/kimg   | Mem.    |
| Baseline                                  | 12.56 s       | 3.10 GB | 18.78 s      | 7.45 GB | 213 s    | 29.7 GB |
| SD-GAN <sub>L<sub>1</sub></sub>           | 14.09 s       | 3.36 GB | 22.20 s      | 8.81 GB |          |         |
| SD-GAN                                    | 19.93 s       | 5.00 GB | 28.33 s      | 9.38 GB | 233 s    | 31.8 GB |
| SD-GAN <sub>L<sub>1</sub></sub> overheads | +12.2%        | +8.4%   | +18.2%       | +18.3%  |          |         |
| SD-GAN overheads                          | +58.7%        | +61.3%  | +50.9%       | +25.9%  | +9.4%    | +7.1%   |

## 4.2 Ablations

Figure 5 compares, for the ProjectedGAN applied to FFHQ at 128<sup>2</sup>, the learning dynamics of the complete SD-GAN to its ablations obtained by disabling augmentations (SD-GAN *w/o. aug.*) or replacing the LPIPS-based  $\mathcal{L}_{SD}$  with simpler distillation losses, which directly compare the images produced by  $G$  and  $G_{EMA}$ :  $L_1$ ,  $L_2$ , and Multi-Scale Structural Similarity Index Measure (MS-SSIM, [47]). Combining the latter variants with augmentations would be pointless, so we do not engage them. The figure presents the averages of 3 runs with shaded standard deviations. While the FID values still fluctuate quite significantly, the LPIPS variants quite clearly converge at the fastest pace, and the augmentations have slight positive impact.

## 4.3 The interplay between loss components

To better understand the interplay between the adversarial and self-distillation objectives, we analyze the visual characteristics of the images favored by each loss component. In Fig. 6, we juxtapose selected images obtained by querying the final  $G_{EMA}$  models on a sample of 10k latent vectors. For each latent, we generate images using both  $G_{EMA}$  and the active generator  $G$ , compute the LPIPS distance  $\mathcal{L}_{SD}$  between them, and select the 200 images with the largest and smallest  $\mathcal{L}_{SD}$  (respectively top and bottom row in the figure). Then we query the discriminator on the  $G_{EMA}$  outputs and select the 4 highest and lowest scoring images, placing them respectively in the right and left quadrants. The figure presents thus the extremes of the joint distribution of  $\mathcal{L}_{SD}$  (vertical) and  $\mathcal{L}_{adv}$  (horizontal), and shows that they exert distinct forces on the generated images. Specifically, the images with worse

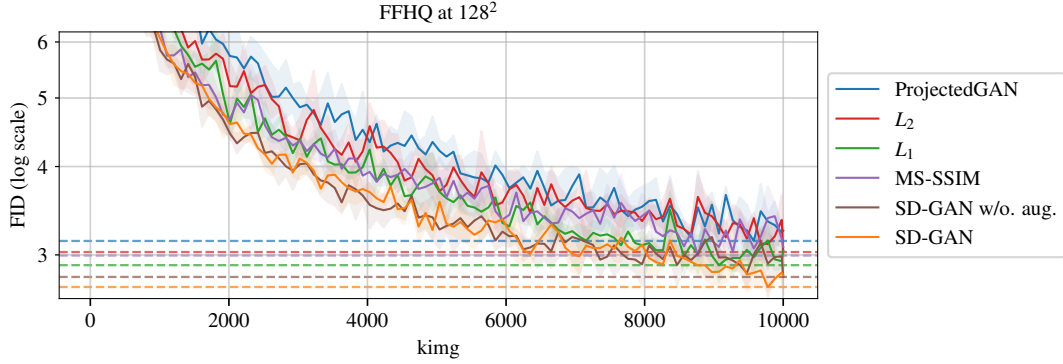
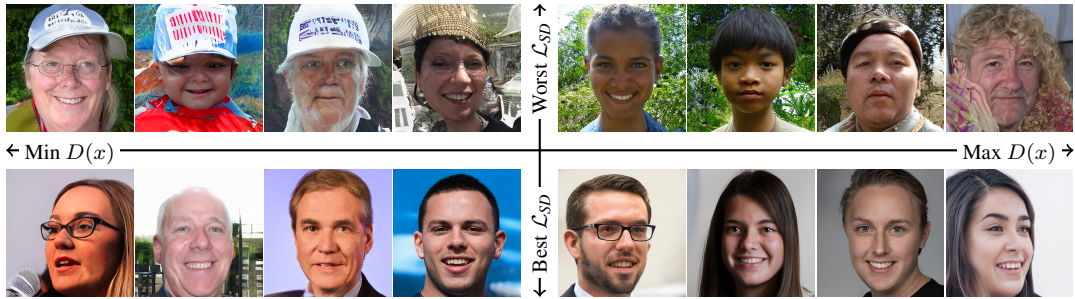
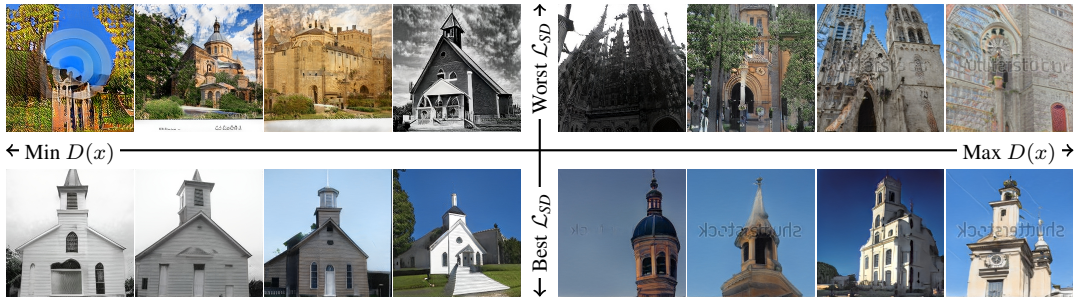


Figure 5: Learning curves for SD-GAN and its ablated variants.



(a) StyleGAN2-ADA+SD, FFHQ at  $256^2$ .



(b) StyleGAN2-ADA+SD, LSUN Church at  $256^2$ .

Figure 6: Qualitative interplay between the objectives. **Left vs. right:** smaller vs. larger *realness* according to  $D$ . **Top vs. bottom:** larger vs. smaller difference between  $G$  and  $G_{EMA}$  (smaller  $\mathcal{L}_{SD}$ ). The adversarial objective pulls generator to the right, while the self-distillation objective pulls it to the bottom. See Fig. 8 for per-image values of  $\mathcal{L}_{SD}$  and  $D$ .

$\mathcal{L}_{SD}$  (top rows) exhibit high-frequency variations, complex backgrounds, and structural artifacts. Minimizing this self-distillation distance (bottom rows) yields remarkably cleaner compositions. Meanwhile, the discriminator (right columns) enforces photorealistic textures and high fidelity, even on detailed images, and its score correlates with image quality, as noted in [48, 49].

#### 4.4 Evolution of generated samples

To quantify the stabilizing effect of the self-distillation objective, we measure the perceptual distance of the StyleGAN2-ADA generators across different training checkpoints (from 20% to 100% kimg) using fixed latent codes. This metric functions similarly to the Perceptual Path Length [15] but is measured across the training trajectory, rather than through latent space interpolation. Table 3 reports the average perceptual distance and its standard deviation of the generated samples across these checkpoints, calculated using a sample size of 480. SD-GAN significantly reduces the perceptual variance between samples compared to the baselines.



Figure 7: Evolution of generated images for a fixed latent vector  $z$  during training. Top two rows: StyleGAN2-ADA; bottom two rows: StyleGAN2-ADA+SD. See Figure 9 for more.

To illustrate the visual effect of the above stabilization, in Fig. 7 we present the evolution of generated images for a fixed latent vector  $z$  throughout the training process, for the sequences whose average perceptual distance is closest to the mean value reported in Table 3. The images generated by the baseline model exhibit very high variance throughout the run; the facial features and church architecture change drastically. In contrast, the face generated by SD-GAN for  $z$  remains relatively stable, and could likely be identified as the same person in all shown images. Similarly, the overall structure of the church is quite consistent.

#### 4.5 Limitations

We identify the following limitations: (i) The LPIPS-based  $\mathcal{L}_{SD}$  may entrench ImageNet-induced biases and lead to “feature pollution”. Though the results on the rFID metric in Table 1 partially alleviate this concern, an even better mitigation of this bias is the choice of non-perceptual losses, which do not seem to lag far behind, as shown in ablations in Fig. 5. (ii) Our empirical evaluation covers three representative GAN architectures and two datasets; broader validation across additional GAN families, datasets, and resolutions remains future work. Though the theoretical analysis and proof of convergence in Sec. 3 suggest that extending the EMA blueprint with self-distillation for GAN training can be universally beneficial, further work is required in order to verify this approach on other GAN-like architectures. (iii) Finally, SD-GAN imposes relatively high computational overhead on training, especially when using perceptual  $\mathcal{L}_{SD}$ . Again, turning to non-perceptual SD losses may alleviate this problem. One may also consider using the same backbone for both the discriminator and the perceptual loss, which would allow querying it only once.

## 5 Conclusions

While nowadays it is diffusion models, rather than GANs, that are the primary tools for image generation, they are often computationally very demanding during inference. Distilling diffusion models into GANs has thus become a common technique to address this deficiency [33, 34, 35]. This makes SD-GAN a potentially useful tool for aiding this process, e.g. fine-tuning the GAN models distilled from diffusion models.

Table 3: Average variation of generated samples across training checkpoints.

| Model         | FFHQ              |                   | LSUN Church       |                   |
|---------------|-------------------|-------------------|-------------------|-------------------|
|               | Baseline          | SD-GAN            | Baseline          | SD-GAN            |
| StyleGAN2-ADA | $0.375 \pm 0.020$ | $0.295 \pm 0.028$ | $0.482 \pm 0.016$ | $0.358 \pm 0.033$ |
| ProjectedGAN  | $0.470 \pm 0.028$ | $0.411 \pm 0.022$ | $0.513 \pm 0.030$ | $0.472 \pm 0.029$ |

## References

- [1] Ian J. Goodfellow, Jean Pouget-Abadie, Mehdi Mirza, Bing Xu, David Warde-Farley, Sherjil Ozair, Aaron Courville, and Yoshua Bengio. Generative adversarial nets. In: *Proceedings of the 28th International Conference on Neural Information Processing Systems*. Vol. 2. Cambridge, MA, USA: MIT Press, 2014, pp. 2672–2680.
- [2] Lars M. Mescheder, Andreas Geiger, and Sebastian Nowozin. Which Training Methods for GANs do actually Converge? In: *Proceedings of the 35th International Conference on Machine Learning, ICML 2018, Stockholmsmässan, Stockholm, Sweden, July 10-15, 2018*. Ed. by Jennifer G. Dy and Andreas Krause. Proceedings of Machine Learning Research. PMLR, 2018, pp. 3478–3487.
- [3] Pavel Izmailov, Dmitrii Podoprikin, Timur Garipov, Dmitry P. Vetrov, and Andrew Gordon Wilson. Averaging Weights Leads to Wider Optima and Better Generalization. In: *Proceedings of the Thirty-Fourth Conference on Uncertainty in Artificial Intelligence, UAI 2018, Monterey, California, USA, August 6-10, 2018*. Ed. by Amir Globerson and Ricardo Silva. AUAI Press, 2018, pp. 876–885.
- [4] Antti Tarvainen and Harri Valpola. Mean teachers are better role models: Weight-averaged consistency targets improve semi-supervised deep learning results. In: *Proceedings of the 31st International Conference on Neural Information Processing Systems*. Red Hook, NY, USA: Curran Associates Inc., 2017, pp. 1195–1204. ISBN: 978-1-5108-6096-4.
- [5] Jean-Bastien Grill, Florian Strub, Florent Altché, Corentin Tallec, Pierre H. Richemond, Elena Buchatskaya, Carl Doersch, Bernardo Avila Pires, Zhaohan Daniel Guo, Mohammad Gheshlaghi Azar, Bilal Piot, Koray Kavukcuoglu, Rémi Munos, and Michal Valko. Bootstrap your own latent a new approach to self-supervised learning. In: *Proceedings of the 34th International Conference on Neural Information Processing Systems. NIPS '20*. Red Hook, NY, USA: Curran Associates Inc., 2020, pp. 21271–21284. ISBN: 978-1-71382-954-6.
- [6] Mathilde Caron, Hugo Touvron, Ishan Misra, Hervé Jégou, Julien Mairal, Piotr Bojanowski, and Armand Joulin. Emerging Properties in Self-Supervised Vision Transformers. In: Proceedings of the IEEE/CVF International Conference on Computer Vision (ICCV). 2021, pp. 9650–9660.
- [7] Maxime Oquab, Timothée Darcet, Théo Moutakanni, Huy V. Vo, Marc Szafraniec, Vasil Khalidov, Pierre Fernandez, Daniel Haziza, Francisco Massa, Alaaeldin El-Nouby, Mido Assran, Nicolas Ballas, Wojciech Galuba, Russell Howes, Po-Yao Huang, Shang-Wen Li, Ishan Misra, Michael Rabbat, Vasu Sharma, Gabriel Synnaeve, Hu Xu, Hervé Jégou, Julien Mairal, Patrick Labatut, Armand Joulin, and Piotr Bojanowski. DINOv2: Learning Robust Visual Features without Supervision. In: *Trans. Mach. Learn. Res.* 2024 (2024).
- [8] Oriane Siméoni, Huy V. Vo, Maximilian Seitzer, Federico Baldassarre, Maxime Oquab, Cijo Jose, Vasil Khalidov, Marc Szafraniec, Seung Eun Yi, Michaël Ramamonjisoa, Francisco Massa, Daniel Haziza, Luca Wehrstedt, Jianyuan Wang, Timothée Darcet, Théo Moutakanni, Leonel Sentana, Claire Roberts, Andrea Vedaldi, Jamie Tolan, John Brandt, Camille Couprie, Julien Mairal, Hervé Jégou, Patrick Labatut, and Piotr Bojanowski. DINOv3. In: *CoRR* abs/2508.10104 (2025). DOI: [10.48550/ARXIV.2508.10104](https://doi.org/10.48550/ARXIV.2508.10104). arXiv: [2508.10104](https://arxiv.org/abs/2508.10104).
- [9] Richard Zhang, Phillip Isola, Alexei A. Efros, Eli Shechtman, and Oliver Wang. The Unreasonable Effectiveness of Deep Features as a Perceptual Metric. In: *Proceedings of the IEEE Conference on Computer Vision and Pattern Recognition (CVPR)*. 2018, pp. 586–595.
- [10] Tim Salimans, Ian Goodfellow, Wojciech Zaremba, Vicki Cheung, Alec Radford, and Xi Chen. Improved techniques for training GANs. In: *Proceedings of the 30th International Conference on Neural Information Processing Systems*. Red Hook, NY, USA: Curran Associates Inc., 2016, pp. 2234–2242. ISBN: 978-1-5108-3881-9.
- [11] Tero Karras, Timo Aila, Samuli Laine, and Jaakko Lehtinen. Progressive Growing of GANs for Improved Quality, Stability, and Variation. In: *6th International Conference on Learning Representations, ICLR 2018, Vancouver, BC, Canada, April 30 - May 3, 2018, Conference Track Proceedings*. OpenReview.net, 2018.
- [12] Yasin Yazici, Chuan-Sheng Foo, Stefan Winkler, Kim-Hui Yap, Georgios Piliouras, and Vijay Chandrasekhar. The Unusual Effectiveness of Averaging in GAN Training. In: *7th International Conference on Learning Representations, ICLR 2019, New Orleans, LA, USA, May 6-9, 2019*. OpenReview.net, 2019.
- [13] Daniel Morales-Brotons, Thijs Vogels, and Hadrien Hendriks. Exponential Moving Average of Weights in Deep Learning: Dynamics and Benefits. In: *Trans. Mach. Learn. Res.* 2024 (2024).

- [14] Andrew Brock, Jeff Donahue, and Karen Simonyan. Large Scale GAN Training for High Fidelity Natural Image Synthesis. In: *7th International Conference on Learning Representations, ICLR 2019, New Orleans, LA, USA, May 6-9, 2019*. OpenReview.net, 2019.
- [15] Tero Karras, Samuli Laine, and Timo Aila. A Style-Based Generator Architecture for Generative Adversarial Networks. In: *Proceedings of the IEEE/CVF Conference on Computer Vision and Pattern Recognition (CVPR)*. 2019, pp. 4401–4410.
- [16] Tero Karras, Samuli Laine, Miika Aittala, Janne Hellsten, Jaakko Lehtinen, and Timo Aila. Analyzing and Improving the Image Quality of StyleGAN. In: *Proceedings of the IEEE/CVF Conference on Computer Vision and Pattern Recognition (CVPR)*. 2020, pp. 8110–8119.
- [17] Tero Karras, Miika Aittala, Janne Hellsten, Samuli Laine, Jaakko Lehtinen, and Timo Aila. Training generative adversarial networks with limited data. In: *Proceedings of the 34th International Conference on Neural Information Processing Systems*. Red Hook, NY, USA: Curran Associates Inc., 2020, pp. 12104–12114. ISBN: 978-1-71382-954-6.
- [18] Tero Karras, Miika Aittala, Samuli Laine, Erik Härkönen, Janne Hellsten, Jaakko Lehtinen, and Timo Aila. Alias-free generative adversarial networks. In: *Proceedings of the 35th International Conference on Neural Information Processing Systems. NIPS '21*. Red Hook, NY, USA: Curran Associates Inc., 2021, pp. 852–863. ISBN: 978-1-71384-539-3.
- [19] Axel Sauer, Kashyap Chitta, Jens Müller, and Andreas Geiger. Projected GANs converge faster. In: *Proceedings of the 35th International Conference on Neural Information Processing Systems*. Red Hook, NY, USA: Curran Associates Inc., 2021, pp. 17480–17492. ISBN: 978-1-71384-539-3.
- [20] Axel Sauer, Katja Schwarz, and Andreas Geiger. StyleGAN-XL: Scaling StyleGAN to Large Diverse Datasets. In: *ACM SIGGRAPH 2022 Conference Proceedings. SIGGRAPH '22*. New York, NY, USA: Association for Computing Machinery, 2022, pp. 1–10. ISBN: 978-1-4503-9337-9. DOI: [10.1145/3528233.3530738](https://doi.org/10.1145/3528233.3530738).
- [21] Axel Sauer, Tero Karras, Samuli Laine, Andreas Geiger, and Timo Aila. StyleGAN-T: unlocking the power of GANs for fast large-scale text-to-image synthesis. In: *Proceedings of the 40th International Conference on Machine Learning*. Vol. 202. ICML'23. Honolulu, Hawaii, USA: JMLR.org, 2023, pp. 30105–30118.
- [22] Yuhta Takida, Masaaki Imaizumi, Takashi Shibuya, Chieh-Hsin Lai, Toshimitsu Uesaka, Naoki Murata, and Yuki Mitsufuji. SAN: Inducing Metrizable of GAN with Discriminative Normalized Linear Layer. In: *The Twelfth International Conference on Learning Representations, ICLR 2024, Vienna, Austria, May 7-11, 2024*. OpenReview.net, 2024.
- [23] Steven Walton, Ali Hassani, Xingqian Xu, Zhangyang Wang, and Humphrey Shi. Efficient Image Generation with Variadic Attention Heads. In: *Proceedings of the IEEE/CVF Conference on Computer Vision and Pattern Recognition (CVPR) Workshops*. 2025, pp. 3264–3275.
- [24] Jonathan Ho, Ajay Jain, and Pieter Abbeel. Denoising diffusion probabilistic models. In: *Proceedings of the 34th International Conference on Neural Information Processing Systems. NIPS '20*. Red Hook, NY, USA: Curran Associates Inc., 2020, pp. 6840–6851. ISBN: 978-1-71382-954-6.
- [25] Yang Song, Jascha Sohl-Dickstein, Diederik P. Kingma, Abhishek Kumar, Stefano Ermon, and Ben Poole. Score-Based Generative Modeling through Stochastic Differential Equations. In: *9th International Conference on Learning Representations, ICLR 2021, Virtual Event, Austria, May 3-7, 2021*. OpenReview.net, 2021.
- [26] Prafulla Dhariwal and Alex Nichol. Diffusion models beat GANs on image synthesis. In: *Proceedings of the 35th International Conference on Neural Information Processing Systems. NIPS '21*. Red Hook, NY, USA: Curran Associates Inc., 2021, pp. 8780–8794. ISBN: 978-1-71384-539-3.
- [27] Han Zhang, Zizhao Zhang, Augustus Odena, and Honglak Lee. Consistency Regularization for Generative Adversarial Networks. In: *8th International Conference on Learning Representations, ICLR 2020, Addis Ababa, Ethiopia, April 26-30, 2020*. OpenReview.net, 2020.
- [28] Long Zhao, Zizhao Zhang, Ting Chen, Dimitris N. Metaxas, and Han Zhang. Improved transformer for high-resolution GANs. In: *Proceedings of the 35th International Conference on Neural Information Processing Systems. NIPS '21*. Red Hook, NY, USA: Curran Associates Inc., 2021, pp. 18367–18380. ISBN: 978-1-7138-4539-3.
- [29] Shengyu Zhao, Zhijian Liu, Ji Lin, Jun-Yan Zhu, and Song Han. Differentiable augmentation for data-efficient GAN training. In: *Proceedings of the 34th International Conference on Neural Information Processing Systems. NIPS '20*. Red Hook, NY, USA: Curran Associates Inc., 2020, pp. 7559–7570. ISBN: 978-1-7138-2954-6.

- [30] Hung-Yu Tseng, Lu Jiang, Ce Liu, Ming-Hsuan Yang, and Weilong Yang. Regularizing Generative Adversarial Networks Under Limited Data. In: *IEEE Conference on Computer Vision and Pattern Recognition, CVPR 2021, virtual, June 19-25, 2021*. Computer Vision Foundation / IEEE, 2021, pp. 7921–7931. DOI: [10.1109/CVPR46437.2021.00783](https://doi.org/10.1109/CVPR46437.2021.00783).
- [31] Shaojie Li, Jie Wu, Xuefeng Xiao, Fei Chao, Xudong Mao, and Rongrong Ji. Revisiting discriminator in GAN compression: a generator-discriminator cooperative compression scheme. In: *Proceedings of the 35th International Conference on Neural Information Processing Systems. NIPS '21*. Red Hook, NY, USA: Curran Associates Inc., 2021, pp. 28560–28572. ISBN: 978-1-7138-4539-3.
- [32] Yuxi Ren, Jie Wu, Xuefeng Xiao, and Jianchao Yang. Online Multi-Granularity Distillation for GAN Compression. In: *Proceedings of the IEEE/CVF International Conference on Computer Vision (ICCV)*. 2021, pp. 6793–6803.
- [33] Axel Sauer, Dominik Lorenz, Andreas Blattmann, and Robin Rombach. Adversarial Diffusion Distillation. In: *Computer Vision – ECCV 2024: 18th European Conference, Milan, Italy, September 29–October 4, 2024, Proceedings, Part LXXXVI*. Berlin, Heidelberg: Springer-Verlag, 2024, pp. 87–103. ISBN: 978-3-031-73015-3. DOI: [10.1007/978-3-031-73016-0\\_6](https://doi.org/10.1007/978-3-031-73016-0_6).
- [34] Axel Sauer, Frederic Boesel, Tim Dockhorn, Andreas Blattmann, Patrick Esser, and Robin Rombach. Fast High-Resolution Image Synthesis with Latent Adversarial Diffusion Distillation. In: *SIGGRAPH Asia 2024 Conference Papers, SA 2024, Tokyo, Japan, December 3-6, 2024*. Ed. by Takeo Igarashi, Ariel Shamir, and Hao (Richard) Zhang. ACM, 2024, 106:1–106:11. DOI: [10.1145/3680528.3687625](https://doi.org/10.1145/3680528.3687625).
- [35] Minguk Kang, Richard Zhang, Connelly Barnes, Sylvain Paris, Suha Kwak, Jaesik Park, Eli Shechtman, Jun-Yan Zhu, and Taesung Park. Distilling Diffusion Models Into Conditional GANs. In: *Computer Vision – ECCV 2024: 18th European Conference, Milan, Italy, September 29–October 4, 2024, Proceedings, Part XXVIII*. Berlin, Heidelberg: Springer-Verlag, 2024, pp. 428–447. ISBN: 978-3-031-73389-5. DOI: [10.1007/978-3-031-73390-1\\_25](https://doi.org/10.1007/978-3-031-73390-1_25).
- [36] Yuanfeng Zheng, Yuchen Yan, and Hao Jiang. Semi-TSGAN: Semi-Supervised Learning for Highlight Removal Based on Teacher-Student Generative Adversarial Network. In: *Sensors* 24.10 (Jan. 2024), p. 3090. ISSN: 1424-8220. DOI: [10.3390/s24103090](https://doi.org/10.3390/s24103090).
- [37] Yang Song, Prafulla Dhariwal, Mark Chen, and Ilya Sutskever. Consistency models. In: *Proceedings of the 40th International Conference on Machine Learning*. Vol. 202. ICML'23. Honolulu, Hawaii, USA: JMLR.org, 2023, pp. 32211–32252.
- [38] Ron Mokady, Omer Tov, Michal Yarom, Oran Lang, Inbar Mosseri, Tali Dekel, Daniel Cohen-Or, and Michal Irani. Self-Distilled StyleGAN: Towards Generation from Internet Photos. In: *ACM SIGGRAPH 2022 Conference Proceedings*. SIGGRAPH '22. New York, NY, USA: Association for Computing Machinery, 2022, pp. 1–9. ISBN: 978-1-4503-9337-9. DOI: [10.1145/3528233.3530708](https://doi.org/10.1145/3528233.3530708).
- [39] Hassan K. Khalil. *Nonlinear Systems*. 2nd. Upper Saddle River, NJ: Prentice-Hall, 1996. ISBN: 978-0-13-228024-2.
- [40] Lars Mescheder, Sebastian Nowozin, and Andreas Geiger. The numerics of GANs. In: *Proceedings of the 31st International Conference on Neural Information Processing Systems. NIPS'17*. Red Hook, NY, USA: Curran Associates Inc., 2017, pp. 1823–1833. ISBN: 978-1-5108-6096-4.
- [41] Vaishnavh Nagarajan and J. Zico Kolter. Gradient descent GAN optimization is locally stable. In: *Proceedings of the 31st International Conference on Neural Information Processing Systems. NIPS'17*. Red Hook, NY, USA: Curran Associates Inc., 2017, pp. 5591–5600. ISBN: 978-1-5108-6096-4.
- [42] Fisher Yu, Ari Seff, Yinda Zhang, Shuran Song, Thomas Funkhouser, and Jianxiong Xiao. *LSUN: Construction of a Large-scale Image Dataset using Deep Learning with Humans in the Loop*. June 4, 2016. DOI: [10.48550/arXiv.1506.03365](https://doi.org/10.48550/arXiv.1506.03365). arXiv: [1506.03365](https://arxiv.org/abs/1506.03365) [cs].
- [43] Martin Heusel, Hubert Ramsauer, Thomas Unterthiner, Bernhard Nessler, and Sepp Hochreiter. GANs trained by a two time-scale update rule converge to a local nash equilibrium. In: *Proceedings of the 31st International Conference on Neural Information Processing Systems. NIPS'17*. Red Hook, NY, USA: Curran Associates Inc., 2017, pp. 6629–6640. ISBN: 978-1-5108-6096-4.
- [44] George Stein, Jesse C. Cresswell, Rasa Hosseinzadeh, Yi Sui, Brendan Leigh Ross, Valentin Vilecroze, Zhaoyan Liu, Anthony L. Caterini, J. Eric T. Taylor, and Gabriel Loaiza-Ganem. Exposing flaws of generative model evaluation metrics and their unfair treatment of diffusion models. In: *Proceedings of the 37th International Conference on Neural Information Processing Systems. NIPS '23*. Red Hook, NY, USA: Curran Associates Inc., 2023, pp. 3732–3784.

- [45] Mehdi S. M. Sajjadi, Olivier Bachem, Mario Lucic, Olivier Bousquet, and Sylvain Gelly. Assessing generative models via precision and recall. In: *Proceedings of the 32nd International Conference on Neural Information Processing Systems*. NIPS'18. Red Hook, NY, USA: Curran Associates Inc., 2018, pp. 5234–5243.
- [46] Ziwei Liu, Ping Luo, Xiaogang Wang, and Xiaoou Tang. Deep Learning Face Attributes in the Wild. In: *Proceedings of the 2015 IEEE International Conference on Computer Vision (ICCV)*. ICCV '15. USA: IEEE Computer Society, 2015, pp. 3730–3738. ISBN: 978-1-4673-8391-2. DOI: [10.1109/ICCV.2015.425](https://doi.org/10.1109/ICCV.2015.425).
- [47] Z. Wang, E.P. Simoncelli, and A.C. Bovik. Multiscale structural similarity for image quality assessment. In: *The Thirty-Seventh Asilomar Conference on Signals, Systems & Computers, 2003*. Vol. 2. 2003, 1398–1402 Vol.2. DOI: [10.1109/ACSSC.2003.1292216](https://doi.org/10.1109/ACSSC.2003.1292216).
- [48] Martin Arjovsky, Soumith Chintala, and Léon Bottou. Wasserstein generative adversarial networks. In: *Proceedings of the 34th International Conference on Machine Learning - Volume 70*. ICML'17. Sydney, NSW, Australia: JMLR.org, 2017, pp. 214–223.
- [49] Samaneh Azadi, Catherine Olsson, Trevor Darrell, Ian J. Goodfellow, and Augustus Odena. Discriminator Rejection Sampling. In: *7th International Conference on Learning Representations, ICLR 2019, New Orleans, LA, USA, May 6-9, 2019*. OpenReview.net, 2019.
- [50] Elad Hoffer, Itay Hubara, and Daniel Soudry. Train longer, generalize better: closing the generalization gap in large batch training of neural networks. In: *Proceedings of the 31st International Conference on Neural Information Processing Systems*. NIPS'17. Red Hook, NY, USA: Curran Associates Inc., 2017, pp. 1729–1739. ISBN: 978-1-5108-6096-4.

## A Software implementation and deployment

The SD-GAN variants used in this study have been implemented by minimally modifying the publicly available ‘official’ implementations of the reference methods:

- StyleGAN2-ADA: <https://github.com/nvlabs/stylegan2-ada-pytorch>
- ProjectedGAN: <https://github.com/autonomousvision/projected-gan>
- StyleNAT: <https://github.com/SHI-Labs/StyleNAT>

The infrastructure consisted of 1 Nvidia H100 GPU, 8 CPU cores, and 32 GB RAM for the single GPU setup and  $4 \times$  Nvidia H100 GPUs, 32 CPU cores and 128 GB RAM for 4 GPU training runs. The total estimated compute we used for all experiments is approximately 10k GPU-hours. The full specification of the nodes we used is:

- CPU: AMD EPYC 9334,  $2 \times 32$  cores
- RAM: 768 GB
- GPU:  $4 \times$  Nvidia H100-94 SXM5, 94GB HBM2e

The official implementation of our proposed method, including training scripts, evaluation routines, and model weights will be available at a later date, accompanied by a supplementary project page featuring animated visualizations.

Typical training runs of SD-GAN using 4 GPUs on the  $256^2$  datasets took respectively 46 h, 20 h, and 14 days for StyleGAN2-ADA+SD, ProjectedGAN+SD, and StyleNAT+SD. In comparison, their respective non-SD baselines took 41 h, 16 h, and 14 days. The baseline runs exhibited runtimes that are close to the SD-GAN runs; this is because, during the baseline experiments, we still explicitly computed the difference between  $G$  and  $G_{EMA}$  (i.e., the  $\mathcal{L}_{SD}$  value) solely for tracking and monitoring purposes, without using it to update the network.

## B Challenges in replication of prior results

Due to the hardware constraints of the Nvidia H100 GPUs (Hopper architecture, `sm_90`) utilized in our experiments, we were required to upgrade PyTorch to ensure compatibility for both StyleGAN2-ADA and ProjectedGAN (compared to the versions used in the original implementations). Specifically, our environment used `torch==2.1.2` compiled with CUDA 12.1.

After several unsuccessful attempts to match the baseline results for StyleNAT on LSUN Church, we excluded this combination from our study. We contacted the authors via a GitHub issue<sup>2</sup>, and while they were very helpful and provided feedback, we ultimately failed to achieve outcomes consistent with the reported benchmarks. It is worth noting that the Church configuration file is missing from their repository, leading us to believe that an omitted or forgotten technical detail may be responsible for the discrepancy.

We also encountered replication challenges with ProjectedGAN. The original work utilized an 8-GPU training setup. In the official implementation in a distributed multi-device setting, Batch Normalization layers compute statistics separately on each device’s mini-batch fragment. This inadvertently applies the concept of *Ghost Batch Normalization* [50], which is known to aid generalization and yield better results than computing statistics over the entire batch. To simulate this 8-GPU dynamic on our 4-GPU setup, we explicitly implemented Ghost BN. However, even with this correction, the best baseline FID we achieved on LSUN Church was 2.11, falling short of the 1.59 reported in the original paper. Furthermore, evaluating the authors’ officially provided model (weights) across various repository commits also failed to reproduce the reported FID. This replication issue appears to be a known problem, mentioned in other independent studies [44] and GitHub issues<sup>3</sup>.

Beyond the specific cases of StyleNAT and ProjectedGAN, we encountered similar replication failures with several other open-source repositories. While we optimistically assume that these discrepancies stem from our own experimental misconfigurations, these repeated challenges serve as a reminder that reproducibility remains a significant issue.

<sup>2</sup><https://github.com/SHI-Labs/StyleNAT/issues/18>

<sup>3</sup><https://github.com/autonomousvision/projected-gan/issues/103>

## C Pseudocode

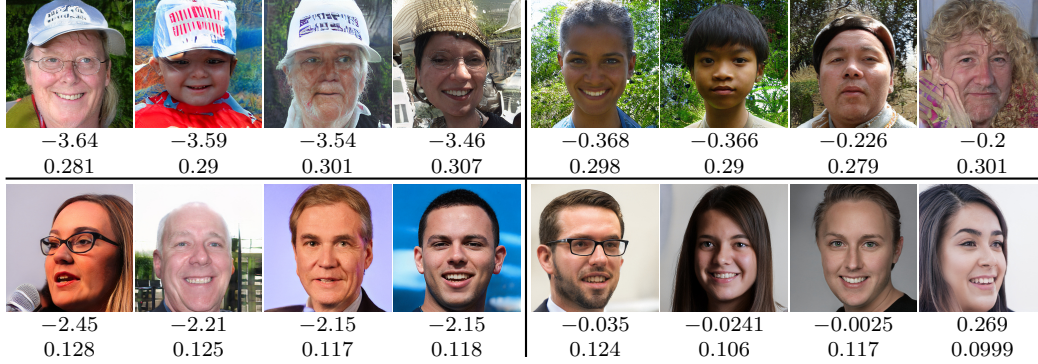
Listing 1 presents the pseudocode of SD-GAN, as implemented in PyTorch.

```
1  loss_type = 'LPIPS'
2  use_aug = True
3  aug2 = AugmentationSequential(
4      RandomHorizontalFlip(p=0.5),
5      RandomRotate(degrees=5, p=0.5),
6      RandomTranslate(translate=(0.01, 0.01), p=0.5),
7      random_apply=2
8  )
9
10 # Inside the training loop:
11 z = torch.randn([batch_size, z_dim])
12 fake_images = G(z)
13 fake_score = D(fake_images)
14 # Normal adversarial loss, e.g.
15 adv_loss = -torch.mean(fake_score)
16 G_loss = adv_loss.mean()
17 # Self-distillation loss
18 with torch.no_grad():
19     fake_images_ema = G_ema(z)
20 if use_aug:
21     fake_images, fake_images_ema = aug2(fake_images, fake_images_ema)
22 if loss_type == 'L1':
23     SD_loss = l1_loss(fake_images, fake_images_ema)
24 elif loss_type == 'LPIPS':
25     SD_loss = lpips(fake_images, fake_images_ema, net='vgg')
26 G_loss = G_loss + alpha * SD_loss.mean()
27 G_loss.backward()
28 # Continue training loop
```

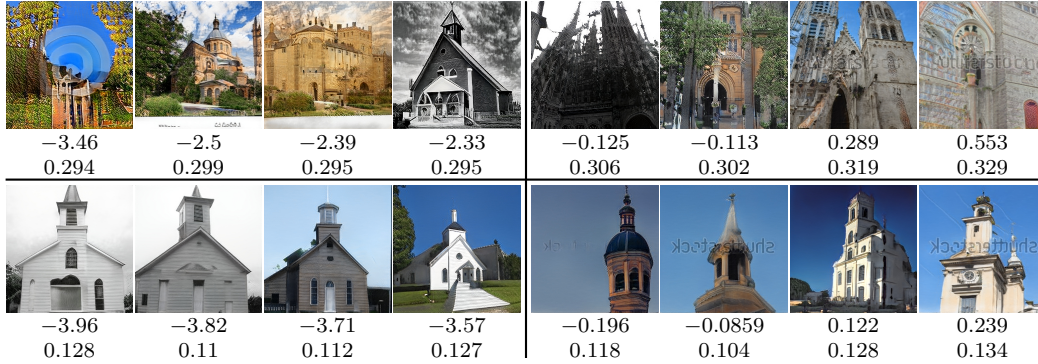
Listing 1: PyTorch pseudocode for the SD-GAN generator update step. The highlighted section demonstrates the calculation of the self-distillation loss.

## D Auxiliary results

Figure 8 presents the detailed version of Figure 6, with additional information on both objectives. The evolution of generated images for a fixed latent vector  $z$  during training is shown in Figure 9. Figure 10 provides a qualitative comparison of the baseline and SD-GAN after fine-tuning on the FFHQ dataset at  $1024^2$  resolution.



(a) StyleGAN2-ADA+SD, FFHQ at  $256^2$ .



(b) StyleGAN2-ADA+SD, LSUN Church at  $256^2$ .

Figure 8: Qualitative interplay between the objectives (detailed version of Fig. 6). **Left vs. right:** smaller vs. larger *realness* according to  $D$  ( $D$  logits, top value). **Top vs. bottom:** larger vs. smaller difference between  $G$  and  $G_{EMA}$  ( $\mathcal{L}_{SD}$ , bottom value under image). The adversarial objective pulls generator to the right, while the self-distillation objective pulls it to the bottom. Best viewed when zoomed in.



(a) StyleGAN2-ADA (FFHQ)



(b) StyleGAN2-ADA+SD (FFHQ)



(c) StyleGAN2-ADA (LSUN Church)

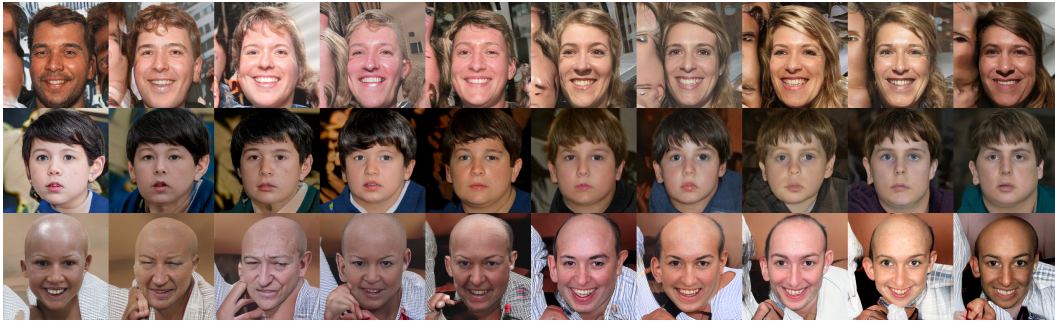


(d) StyleGAN2-ADA+SD (LSUN Church)

Figure 9: Evolution of generated images for a fixed latent vector  $z$  during training. (Continued on next page)



(e) ProjectedGAN (FFHQ)



(f) ProjectedGAN+SD (FFHQ)



(g) ProjectedGAN (LSUN Church)



(h) ProjectedGAN+SD (LSUN Church)

Figure 9: Evolution of generated images for a fixed latent vector  $z$  during training. The progressions are grouped by model and dataset (detailed version of Figure 7).



(a) StyleGAN2-ADA (FFHQ 1024<sup>2</sup> fine-tuning)



(b) StyleGAN2-ADA+SD (FFHQ 1024<sup>2</sup> fine-tuning)

Figure 10: Qualitative results after fine-tuning on FFHQ at 1024<sup>2</sup>. Samples generated using the same latent vectors for both methods are shown for comparison.